

James N. Marquis* and Yvette P. Richardson
 Pennsylvania State University, University Park, PA,
 Joshua M. Wurman
 Center for Severe Weather Research, Boulder, CO

1. INTRODUCTION

Misocyclones are vortices in the horizontal plane with diameters $< 4\text{km}$ (Fujita, 1981). They are often found along boundaries with horizontal shearing instability (Wakimoto and Wilson, 1989) such as the leading edge of thunderstorm outflows (Fujita 1981, Mueller and Carbone 1987), cold fronts (Wilson 1986), drylines, and other lines of convergence associated with a wind shift (Wilson et al., 1992; Crook et al. 1991).

The presence of misocyclones along a boundary often corresponds to enhanced vertical motion directly to the north and northwest of the misocyclone and to the south and southeast of the misocyclone (for a north to south oriented boundary). Because of this modified vertical motion, misocyclones are thought to play a role in convection initiation (Weckwerth and Wakimoto 1992, Kingsmill 1995, Wilson et al. 1992), therefore, understanding their structure and behavior was one goal of the International H₂O Project (IHOP) (Weckwerth et al., 2004). Additionally, misocyclones have been shown to play a key role in the generation of non-supercell tornadoes (Carbone 1982, 1983, Lee and Wilhelmson 1997b).

Detailed observations of misocyclones are rare, especially those with temporal continuity sufficient to verify numerical modeling studies and to show any relationship between misocyclone characteristics and boundary organization. This study focuses on high temporal and spatial resolution radar observations of misocyclones along three surface boundaries targeted during IHOP. Section 2 provides background information regarding misocyclones as determined from other studies. Section 3 briefly describes the three data sets and the field instruments used in each for purposes of this study. Section 4 documents: 1) the properties of a typical misocyclone from all three data sets 2) the size, distribution, and motion of misocyclones along the boundaries, and 3) mergers of misocyclones. A key example of each is presented.

2. BACKGROUND

Misocyclones shown in past studies possess rotation that is strongest at the ground and decreases with height. It is common for ‘S’ shapes or whirls to

occur in radar reflectivity along the boundary where a misocyclone is located (Carbone, 1982; Wilson, 1986; Mueller and Carbone, 1987; Wakimoto and Wilson, 1989) because the misocyclone circulates air east of the boundary around its northern periphery and air west of the boundary around its southern periphery (assuming cyclonic rotation and a north to south oriented boundary).

Lee and Wilhelmson (1997a) (hereafter LW97a) provide a thorough survey of the intensification, motion, mergers, and decay of a population of misocyclones forming at inflections points on a simulated outflow boundary. The number of misocyclones present in their domain decreases in time due to interactions (including mergers), with the diameter of each remaining vortex increasing prior to decay. Such a population exhibits the following behavior. Initially, discrete vortices are produced from a linear zone of vorticity along the wind shift boundary (“vortex sheet roll up” stage). These small, discrete misocyclones then tend to pair up and interact (“subharmonic interaction” stage). In the next stage, paired vortices either merge or one becomes dominant at the expense of the other (“consolidation” stage). The final stage occurs when individual misocyclones decay and the inflections on the edge of the boundary occlude (“dissipation” stage). Misocyclones resulting from the consolidation stage are larger and typically possess values of vertical vorticity (ζ) similar to those of the parent misocyclones. This results in larger value of circulation for the resultant misocyclones.

3. CASE DESCRIPTIONS

Convection initiation (CI) studies during IHOP specifically targeted convergence boundaries, therefore, all three data sets used in this study are CI missions containing detailed misocyclone observations. On 3 June 2002 the Doppler on Wheels 2 and 3 (DOW2 and DOW3) (Wurman 1997) and the X-band Polarimetric (XPOL) (Wurman 2001) mobile radars observed an ENE to WSW oriented cold front in the eastern Oklahoma panhandle. Operations took place from 1500 UTC (all times are UTC) through 0400 20 June. The data used for this study are from 1615 to 2030.

On 10 June 2002 DOW2, DOW3, XPOL, and the Shared Mobile Atmospheric Research and Teaching Radar (SMART-Radar) (Biggerstaff and Guynes 2000) observed a NE to SW oriented quasi-stationary front near Ness City, Kansas. Operations took place from

*Corresponding Author Address: James Marquis, Department of Meteorology, The Pennsylvania State University, University Park, PA 16802; e-mail: jnm128@psu.edu

1600 to 0100; however, data used in this study are limited to those between 1928 and 2118.

On 19 June 2002, DOW2, DOW3, and XPOL observed a NNE to SSW oriented dryline near Colby, Kansas. Mobile radar observations are available from 1921 to 2345, during which time intense misocyclone activity and a non-supercell tornado were observed.

4. SURVEY OF MISOCYCLONES

4.1 Description of an Average Misocyclone

Figure 1 shows a plan view (Fig.1a) and a vertical cross section (Fig.1b) of a misocyclone observed on 10 June 2002 that is characteristic of those in all three data sets. The misocyclone in Fig.1 is located in a radar reflectivity maximum along a portion of the boundary where an ‘S’ shape is present in the reflectivity field. The convergence field surrounding the misocyclone is consistent with that described in section 1, verifying the simulations of LW97a.

The axis of maximum vertical vorticity of most misocyclones in this study is nearly vertical in all stages of growth with the strongest vorticity at the surface (Fig.1b). On rare occasions during the dissipation stage, the region of strongest rotation in a misocyclone is instead found several hundred meters AGL. A tilt in the vertical structure of ζ is most often seen when a misocyclone is in its dissipation stage or is interacting with a neighboring vortex. The vortex in Fig.1 has reached maturity, with a weak downdraft evident in its core. Given the range of this misocyclone from the closest radars (~ 12 km) the lowest beam has a height of approximately 100m and the beam width is approximately 200 m, thus, it is difficult to say whether this downdraft truly reaches the surface. A shallow layer of convergence in the lowest ~ 150 m, consistent with LW97a, cannot be ruled out.

In comparing the three observed boundaries, it appears the average maximum value of ζ in the observed misocyclones may be related to the strength of vertical motion along the boundary. The organization of vertical motion is the most persistent and the peak magnitude of vertical motion is the greatest (~ 8 ms^{-1} at 1 km AGL) along the dryline on 19 June. Misocyclones on this day possess the largest peak ζ (often exceeding $20 \times 10^{-3} \text{ s}^{-1}$ at 100 m AGL) of all three data sets. On 10 June, peak ζ reaches $16 \times 10^{-3} \text{ s}^{-1}$ in several misocyclones and vertical motion fields reach peak values near 5 ms^{-1} at 1 km AGL. Peak vertical motion on 3 June rarely exceeds 2.5 ms^{-1} and the most intense misocyclone on this day reaches a peak ζ just above $10 \times 10^{-3} \text{ s}^{-1}$.

At many times in all three data sets, populations of misocyclones organize the convergence pattern along a portion of the boundary in a “stair-step configuration” of conjoined misocyclone convergence

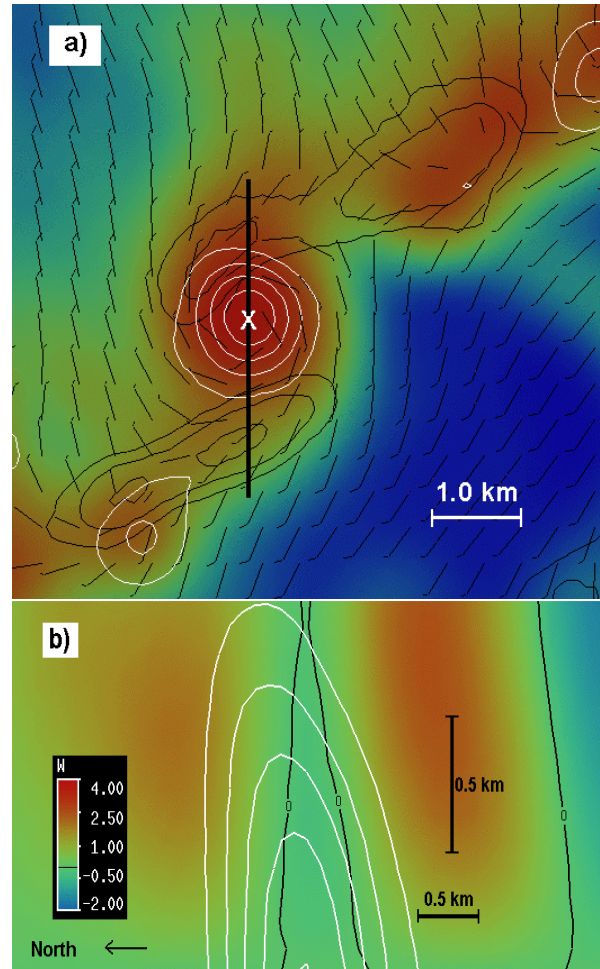


Fig.1. (a) Plan view of a typical misocyclone at 100 m AGL nearing its dissipation stage. DOW2 reflectivity is colored, ζ is contoured in white, convergence is contoured in black, and barbs depict the misocyclone-relative wind. The minimum contour of convergence is $2.5 \times 10^{-3} \text{ s}^{-1}$ with an increment of $+1 \times 10^{-3} \text{ s}^{-1}$. Long wind barb flags are 10 ms^{-1} and short flags are 5 ms^{-1} . The dark line corresponds to the vertical cross section shown in (b). Contours in (b) represent ζ , while colors correspond to radar-determined vertical motion in ms^{-1} . For reference, the black contour is $w = 0.0 \text{ ms}^{-1}$. Note that (b) is stretched in the vertical. The minimum contour of ζ in (a) and (b) is $4 \times 10^{-3} \text{ s}^{-1}$ and the contour increment is $+3 \times 10^{-3} \text{ s}^{-1}$.

regions (as in Fig.1a). An example from 19 June is presented in Fig.2.

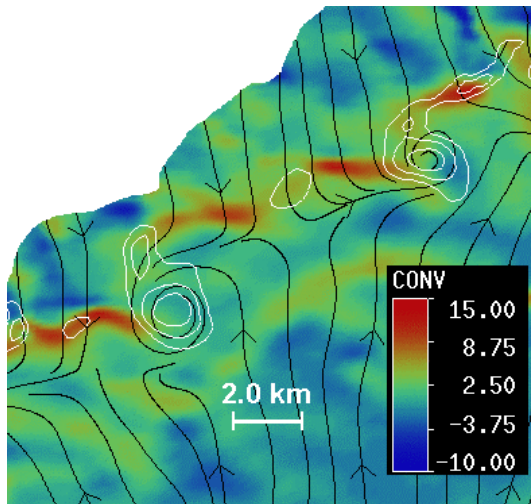


Fig.2 Organization of convergence along a boundary containing a population of misocyclones. Vertical vorticity (ζ) is contoured in white, convergence is shaded in units of $\times 10^{-3} \text{ s}^{-1}$, and streamlines are for wind relative to estimated misocyclone motion. The minimum contour of ζ is $4 \times 10^{-3} \text{ s}^{-1}$, with a contour interval of $+3 \times 10^{-3} \text{ s}^{-1}$.

4.2 Population Evolution

The evolution of a misocyclone population from 2121 to 2225 on 19 June 2002 is presented in Fig.3. All diameters referred to below are with respect to the $7 \times 10^{-3} \text{ s}^{-1}$ vorticity contour at 100 m AGL.

Figure 3a shows the pairing of several small vortices along the boundary with average diameters of 1.1 km. This is consistent with the “subharmonic interaction” stage defined by LW97a. As time progresses, the paired misocyclones merge into vortices with larger diameters (e.g. CD, EF, GH). The resultant misocyclones on the boundary are evenly spaced with an average separation of approximately 4.0 km (Fig.3b). This resembles the “consolidation” stage defined by LW97a. Meanwhile, misocyclones J and K enter the domain from the south.

By 2145 (Fig.3c), EF and IJ have grown in size through mergers with other misocyclones on the boundary and with small ζ patches present outside of the boundary. A large bend on the boundary in the vicinity of IJ and GH corresponds to their westward displacement and a reduction in their northeastward component of propagation. As a result, IJ and K become sufficiently close for effective interaction. Misocyclones L and M enter the domain from the south while A, B, CD, and EF leave the domain to the north by 2157 (Fig.3d). The westward displacement of GH results in a pairing with IJK near 2209 (Fig.3e). Only three misocyclones are in the analysis domain at 2225 (Fig.3f). They are evenly spaced with an average separation of approximately 8.0 km (twice the spacing

of misocyclones in Fig.3b). At 2225 the average circular diameter of GHIJK, LM, and N is 1.8 km, indicating a 60% increase in diameter from the misocyclones in Fig.3a. The increase in both average separation distance and diameter of misocyclones in the population represented in Fig.3 is generally consistent with the increases simulated in a similar population by LW97a.

4.3 Merger Evolution

The merger of misocyclones L and M (from Fig.3) between 2203 and 2234 is shown in Fig.4. While several mergers are observed in this study, this event is prototypical as both L and M are clearly defined, possess intense ζ fields, and the merger proceeds in a region void of other major vorticity maxima.

At 2203 (Fig.4a), each misocyclone has its own associated convergence field, generally similar to that in Fig.1a. The pairing of L and M is evident at 2221 (Fig.4b). While M has maintained its peak value of ζ , the peak ζ of L has decreased, making misocyclone M the dominant vortex. Due to the close proximity of L and M at 2221, the vorticity pattern becomes elongated along the merger axis (line connecting vorticity maxima of each misocyclone). The convergence field takes on a much more complex pattern, with the strongest convergence located south of the merging pair. The ‘S’ shape in reflectivity in Fig.4b, while similar to that associated with an individual misocyclone, is elongated along the merger axis, locally altering the orientation of the boundary. A similar elongated ‘S’ is observed (not shown) at 2212 during the merger of vortices GH and IJK (from Fig.3), with a slightly different orientation. Conversely, when the merger axis is parallel to the boundary or when the original vortices are relatively small (e.g., final vortices CD, EF, GH in Fig. 3), a convergence pattern similar to that of Fig.1a is maintained relative to the pair as a whole.

At 2228 (Fig.4c), L and M have fully consolidated. The elongated ‘S’ in the reflectivity field from Fig.4b has occluded, but a less elongated inflection in radar reflectivity is collocated with LM. While there is no significant difference in the peak ζ of LM (in Fig.4c) versus L or M (in Fig.4a), the diameter of LM is larger than that of L and M. Thus, the circulation of LM is larger than the circulation of either of them individually. This is consistent with LW97a.

5. SUMMARY AND CONCLUSIONS

High resolution dual- and multi-Doppler radar observations of three synoptic boundaries during IHOP documented many misocyclones that verify numerical model simulations and several observational studies regarding structure, behavior, and association with regions of vertical velocity. The strength of vertical

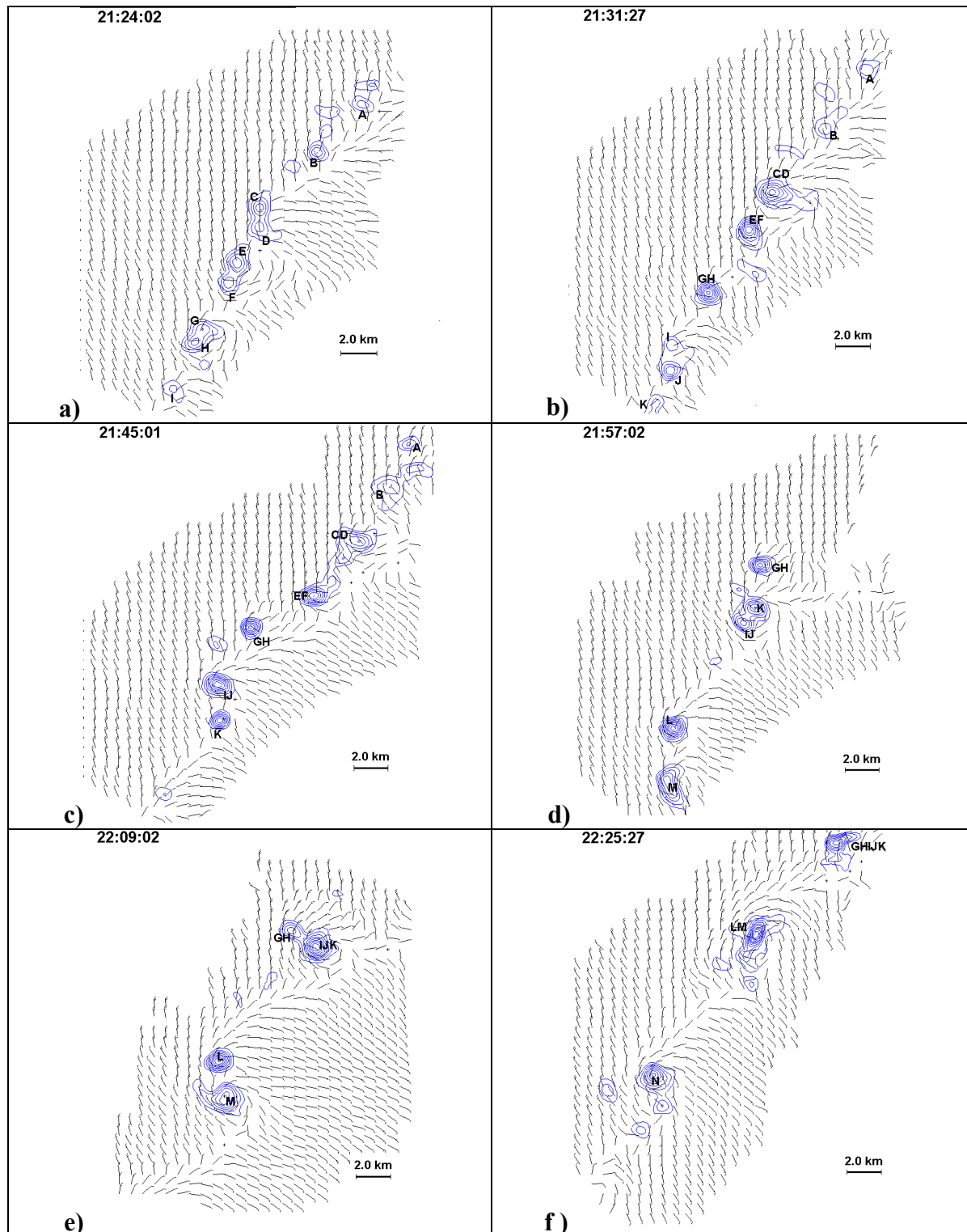


Fig.3. An evolution of a misocyclone population from 2124 to 2225 on 19 June 2002. Individual misocyclones that result from a merger of two or more vortices are labeled with the letters of all vortices involved. Vertical vorticity is contoured in increments of $3.0 \times 10^{-3} \text{ s}^{-1}$ with a minimum contour of $4.0 \times 10^{-3} \text{ s}^{-1}$. Only positive ζ is shown. Barbs are misocyclone relative wind. Long flags are 10 ms^{-1} , short flags are 5 ms^{-1} . Times given are for the start of the ~ 90 second volume.

motion near a misocyclone appears to be related to the intensity of the misocyclone, at least in this limited sample. The strength of the misocyclones and the vertical motion field may depend on larger-scale boundary properties. A misocyclone population containing relatively large vortices with fairly regular spacing is often found to exhibit a “stair-step” pattern of convergence along the boundary. Through a series of “subharmonic interaction” and “consolidation” stages, a population of several small, evenly spaced misocyclones transforms into a population of larger, evenly spaced misocyclones. The merger of a pair of misocyclones produces a larger misocyclone with similar vertical vorticity and greater circulation. This larger circulation often creates more elongated boundary inflections and modified convergence fields compared to smaller misocyclones. The disruption of the original convergence pattern by a merger may depend on the orientation of the merger axis and the size of the misocyclones involved. It is felt that enlarged circulations associated with merging misocyclones might play a unique role in CI by the redistribution of moisture and convergence fields.

6. ACKNOWLEDGEMENTS

This study is funded under NSF grant ATM-0208651. The authors thank: Paul Markowski and Nettie Arnott for the writing of and assistance with radar synthesis scripts, N. Arnott and John Stonitsch for providing radar observations and analysis opinions, and all who aided the collection of the 3, 10, and 19 June 2002 data sets during IHOP. The authors also thank the NCAR/UCAR authors of the REORDER and CEDRIC routines used to produce the wind syntheses.

7. REFERENCES

- Biggerstaff, M. I., and J. Guynes, 2000: A new tool for atmospheric research. *20th Conf. on Severe Local Storms*, Orlando, Amer. Meteor. Soc., 277-280
- Carbone, R.E., 1982. A severe frontal rainband. Part I: Stormwide hydrodynamic structure. *J. Atmos. Sci.*, **39**, 258-279.
- _____, 1983:. A severe frontal rainband. Part II: Tornado parent vortex circulation. *J. Atmos. Sci.*, **40**, 2639-2654.
- Crook, N.A., and M.W. Moncrieff, 1991: The Denver cyclone. Part II: Interaction with the convective boundary layer. *J. Atmos. Sci.*, **48**, 2109-2126.
- Fujita, T.T., 1981: Tornadoes and downbursts in the context of generalized planetary Scales. *J. Atmos. Sci.*, **38**, 1511-1534.
- Kingsmill, D.E., 1995: Convection initiation associated with a sea-breeze front, a gust front, and their collision. *Mon. Wea. Rev.*, **123**, 2913-2933.

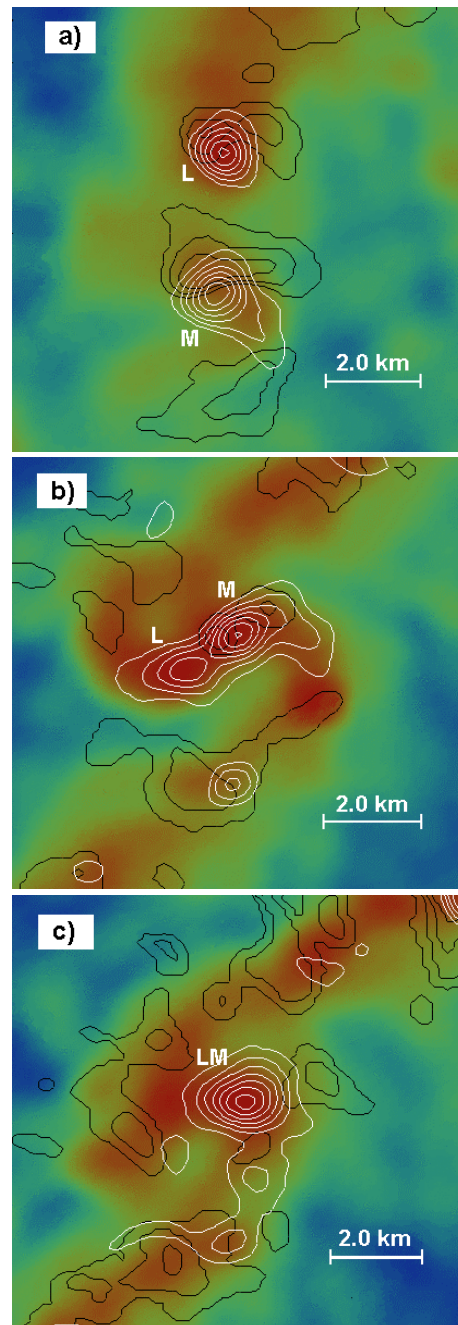


Fig. 4. Evolution of a misocyclone merger at 100 m AGL from 2203(a) to 2228(c) on 19 June 2002. Vertical vorticity (ζ) is contoured in white. The minimum vorticity contour is $4.0 \times 10^{-3} \text{ s}^{-1}$, with a contour interval of $+3.0 \times 10^{-3} \text{ s}^{-1}$. Convergence is contoured in black. The minimum contour in each convergent zone $2.5 \times 10^{-3} \text{ s}^{-1}$, with a contour interval of $+2 \times 10^{-3} \text{ s}^{-1}$. Misocyclones are labeled by letter as they are in Fig.1. DOW2 radar reflectivity (dBZ) is colored.

- Lee, B.D., and R.B. Wilhelmson, 1997a: The numerical simulation of non-supercell tornadogenesis. Part I: Initiation and evolution of pretornadic mesocyclone circulations along a dry outflow boundary. *J. Atmos. Sci.*, **54**, 32-60.
- _____, 1997b: The numerical simulation of non-supercell tornadogenesis. Part II: Evolution of a family of tornadoes along a weak outflow boundary. *J. Atmos. Sci.*, **54**, 2387-2414.
- Mueller, C.K., and R.E. Carbone, 1987: Dynamics of a thunderstorm outflow. *J. Atmos. Sci.*, **44**, 1879-1898.
- Wakimoto, R., and J.W. Wilson, 1989: Non-supercell tornadoes. *Mon. Wea. Rev.*, **117**, 1113-1140.
- Weckwerth, T.M., and R. Wakimoto, 1992: The initiation and organization of convective cells atop a cold-air outflow boundary. *Mon. Wea. Rev.*, **120**, 2169-2187.
- _____, D.B. Parsons, S.E. Koch, J.A. Moore, M.A. LeMone, B.B. Demoz, C. Flamant, B. Geerts, J. Wang, and W.F. Feltz, 2004: An overview of the International H₂O Project (IHOP) and some preliminary highlights. *Bull. Amer. Meteor. Soc.*, **85**, 253-277.
- Wilson, J.W., 1986: Tornadogenesis by nonprecipitation induced by wind shear lines. *Mon. Wea. Rev.*, **114**, 270-284.
- _____, G.B. Foote, N.A. Crook, J.C. Fankhauser, C.G. Wade, J.D. Tuttle, and D.K. Mueller, 1992: The role of boundary-layer convergence zones and horizontal rolls in the initiation of thunderstorms: A case study. *Mon. Wea. Rev.*, **120**, 1785-1815.
- Wurman, J. M., J. Straka, E. Rasmussen, M. Randall, and A. Zahrai, 1997: Design and development of a portable, pencil-beam, pulsed, 3-cm Doppler radar. *J. Atmos. Oceanic Technol.*, **14**, 1502-1512.
- Wurman, J., 2001: The DOW mobile multiple Doppler network. Preprints, 30th International Conf. on Radar Meteorology, Munich, Germany, Amer. Meteor. Soc., 95-97.